Int. J. Electrochem. Sci., 6 **(2011)** 4422 - 4437

International Journal of
ELECTROCHEMICAL
SCIENCE
www.electrochemsci.org

Alcohol Dehydrogenase Immobilized at Cerium Hexacyanoferrate (II) Nanoparticles Incorporated Poly-L-Lysine Film for Voltammetric Ethanol Determination

Arun Prakash Periasamy, Jia–Xuan Wei, Shen-Ming Chen[*]

Department of Chemical Engineering and Biotechnology, National Taipei University of Technology, No.1, Section 3, Chung-Hsiao East Road , Taipei 106, Taiwan (R.O.C).
[*]E-mail: smchen78@ms15.hinet.net

Received: 4 August 2011 / *Accepted:* 28 August 2011 / *Published:* 1 October 2011

We report a voltammetric ethanol sensor based on alcohol dehydrogenase immobilized at cerium hexacyanoferrate (II) (CeHCF(II)) nanoparticles incorporated poly-L-lysine (PLL) film modified glassy carbon electrode (GCE). The electrostatic interactions between PLL, CeHCF(II) nanoparticles and ADH layers provide good stability to the nanocomposite film. The as-prepared CeHCF(II) nanoparticles and ADH/PLL/CeHCF/PLL films were characterized by field emission scanning electron microscopy (FESEM) and atomic force microscopy (AFM) study. FESEM results confirmed that CeHCF(II) nanoparticles are 25–30 nm in size. Powder X-ray diffraction (XRD) results demonstrated that CeHCF(II) nanoparticles are crystalline and belongs to hexagonal symmetry with a space group of $P6_3/m$. The fabricated ADH/PLL/CeHCF/PLL nanocomposite film modified GCE exhibits excellent electrocatalytic response towards ethanol in 0.1 M KNO_3 solution (pH 7). The linear concentration range and sensitivity values are 0.04 to 0.23 mM and 13.86 μA mM^{-1} cm^{-2}, respectively. The proposed ADH/PLL/CeHCF/PLL film exhibits good stability, high selectivity and it detects ethanol present in commercially available red wine samples with good recovery.

Keywords: alcohol dehydrogenase, poly-L-lysine, cerium hexacyanoferrate (II) nanoparticles, ethanol, electrocatalysis.

1. INTRODUCTION

The determination of ethanol from real samples is essential since ethanol has been largely used in food and beverage industries [1, 2]. However, to achieve highly sensitive and selective ethanol quantification, alcohol dehydrogenase (ADH) enzyme based biosensors have been widely used these days [3-4]. The advancements in nanotechnology field and the unique properties of nanostructured materials such as large surface area, high mechanical strength, porous surface morphology and extremely miniaturized size have widened their applications in ADH based biosensors [5-7]. However,

previous studies revealed that inclusion of redox mediators to the biosensor film assembly can decrease the over potential for ethanol determination and it avoids the electrode surface fouling related problems [8, 9]. Earlier Cai et *al.* reported an ADH based biosensor using nickel hexacyanoferrate modified microband gold electrode via covalent cross-linking chemistry for the assay of ethanol [10]. In the past years, several redox dyes have been used for the development of ADH based biosensors [11-13]. Recently, we reported an ADH based biosensor based on the electrostatic interactions between oppositely charged toluidine blue O (TBO), ADH and nafion films to achieve low potential (-0.14 V) ethanol determination [14].

In recent years, synthesis and investigation of the electrochemical behavior of metal hexacyanoferrates (MHCF) have attracted considerable attention due to their highly reversible redox reactions and their ability to mediate number of electrochemical processes. In particular, high stability of the metal cyanide framework in MHCFs and the possibility for cation exchange between a solution and the cages of framework has made their electrochemistry much more interesting [15]. To date, the electrochemistry of several MHCFs has been investigated by many research groups [16, 17]. Along with the significant advancements made in nanotechnology field, MHCF nanoparticles have been successfully synthesized and electrochemically characterized by several researchers [18]. Owing to the large surface area, good conductivity and outstanding catalytic activity, MHCF nanoparticles modified electrodes have been widely employed as versatile tools for electrochemical sensors [19- 21] and biosensors applications [22, 23]. Nevertheless, due to the excellent luminescence property, wide band gap, tunable electronic properties cerium hexacyanoferrate, CeHCF(II) has found its applications in diverse fields. Recently, Feng et *al.* reported the facile electrochemical route using amperometric technique for controllable synthesis of flowerlike and fusiform christmas-tree like CeHCF(II) microparticles [24]. Yang et *al.* have also described the electrochemical preparation of CeHCF(II) film on ordered mesoporous carbon electrode via cyclic voltammetry and reported the electrochemical oxidation of hydrazine [25]. However, to the best of our knowledge no reports are available on the application of electrochemically synthesized CeHCF(II) nanoparticles in ADH based biosensors.

Poly-L-lysine (PLL) is another attractive biocompound which is well known for its biocompatibility. The availability of plentiful positively charged active $–NH_2$ groups in its structural framework can be very useful for the attachment of enzymes and biomolecules above the transducer surface [26]. In the present study, we report the electrochemical synthesis of CeHCF(II) nanoparticles on PLL modified glassy carbon electrode (GCE) via amperometric technique. The electrostatic interactions between the positively charged $–NH_2$ groups of PLL and negatively charged CeHCF(II) nanoparticles adds good stability to the film. In order to construct an ADH based biosensor, a positively charged PLL layer was casted above the CeHCF/PLL film. The resulting PLL/CeHCF/PLL film has been used as a novel immobilization matrix for ADH. The fabricated ADH/PLL/CeHCF/PLL nanocomposite film exhibits excellent electrocatalytic activity towards ethanol with acceptable sensitivity and high selectivity. The proposed ADH based biosensor also detects ethanol from commercial red wine with good recovery, which validates its good practical applicability.

2. EXPERIMENTAL

2.1. Reagents and Apparatus

Cerium (III) nitrate hexahydrate and potassium hexacyanoferrate (III) were purchased from Wako pure chemical Industries, Ltd. Poly-L-lysine hydrobromide (PLL) and alcohol dehydrogenase (ADH) from Saccharomyces cerevisiae were obtained from Sigma. The supporting electrolyte used for all experiments is 0.1 M KNO_3 solution (pH 7). All the reagents used were of analytical grade and doubly distilled water was used for the preparation of all aqueous solutions. Prior to each experiment, the experimental solutions were deoxygenated with pre-purified N_2 gas for 10 min and the N_2 tube was kept above the solutions to maintain an inert atmosphere.

Cyclic voltammetry (CV) and differential pulse voltammetry (DPV) studies were carried out using CHI 410a and CHI 1205a work stations, respectively. A conventional three electrode cell containing 0.1 M KNO_3 solution (pH 7) was used as supporting electrolyte for all the electrochemical studies. For CV studies, glassy carbon electrode (GCE) with a working area of 0.079 cm^2 was used as working electrode. Pt wire with 0.5 mm diameter was used as counter electrode and all the potentials were referred with respect to standard Ag/AgCl reference electrode. EIM6ex ZAHNER (Kroanch, Germany) was used for electrochemical impedance spectroscopy (EIS) studies. Surface morphology of all films was studied using Being nano-instruments CSPM 4000, atomic force microscope (AFM). Field emission scanning electron microscope (FESEM), JSM-6500F was used to investigate the surface morphology of as-prepared CeHCF(II) nanoparticles and the fabricated ADH/PLL/CeHCF/PLL film. Powder X-ray diffraction (XRD) studies were performed in a XPERT-PRO (PANalytical B.V., The Netherlands) diffractometer using Cu K_α radiation (k = 1.54 A °). For AFM, FESEM and powder XRD studies all the films were prepared on indium tin oxide (ITO) electrodes.

2.2 Fabrication of ADH/PLL/CeHCF/PLL film modified GCE

Initially, ADH (5 mg mL^{-1}) and PLL (1 mg mL^{-1}) solutions were prepared separately in 0.1 M KNO_3 solution (pH 7) and were stored in refrigerator at 4 °C, when not in use. GCE surface was polished well on a clean Buehler polishing cloth using 0.05 μm alumina slurry, followed by washing and ultrasonicating the GCE surface in doubly distilled water for 10 min and finally dried at room temperature. The nanocomposite film was fabricated on the pre-cleaned GCE surface in four steps. In step (i) positively charged PLL film was fabricated by drop casting 10 μl of PLL solution on the pre-cleaned GCE surface and drying at 30° C in air oven for 30 min. (ii) Then negatively charged CeHCF(II) nanoparticles were electrochemically deposited on PLL modified GCE surface with slight modification to the procedure reported in literature [24]. In a typical procedure, PLL film modified GCE was immersed in a mixture of 5.0 mM $Ce(NO_3)_3$, 5.0 mM $K_3[Fe(CN)_6]$ and 0.1 M KNO_3 solutions and the electrode potential was kept constant at -0.2 V for 500 s. As-deposited CeHCF(II) nanoparticles modified GCE surface was gently washed with doubly distilled water to remove the

loosely adsorbed CeHCF(II) nanoparticles. The formation of CeHCF(II) nanoparticles on GCE surface can be explained by the reaction mechanism proposed by Feng et. *al.* as shown in equation (1)

$$Fe(CN)_6^{4-} + Ce^{3+} + K^+ + 4H_2O \longrightarrow KCe[Fe(CN)_6] \cdot 4H_2O \quad (1)$$

In step (iii) positively charged PLL film was formed above the negatively charged CeHCF(II) nanoparticles by repeating step (i). Finaly, in step (iv) negatively charged ADH film [27] was assembled over the positively charged PLL film by drop casting 10 µl of ADH (10 mg mL^{-1}) solution and then drying at 30 min for 30° C. Thus prepared ADH/PLL/CeHCF/PLL modified GCE was finally rinsed few times with doubly distilled water to remove the loosely bound ADH. For comparison PLL, PLL/CeHCF films were also fabricated on GCE.

3. RESULTS AND DISCUSSIONS

3.1 Surface morphological characterization studies using FESEM and AFM studies

The surface morphology of as-prepared CeHCF(II) nanoparticles and ADH/PLL/CeHCF/PLL nanocomposite films were investigated by FESEM study. Fig. 1 (A) shows the FESEM image of spherical shaped well distributed CeHCF(II) nanoparticles.

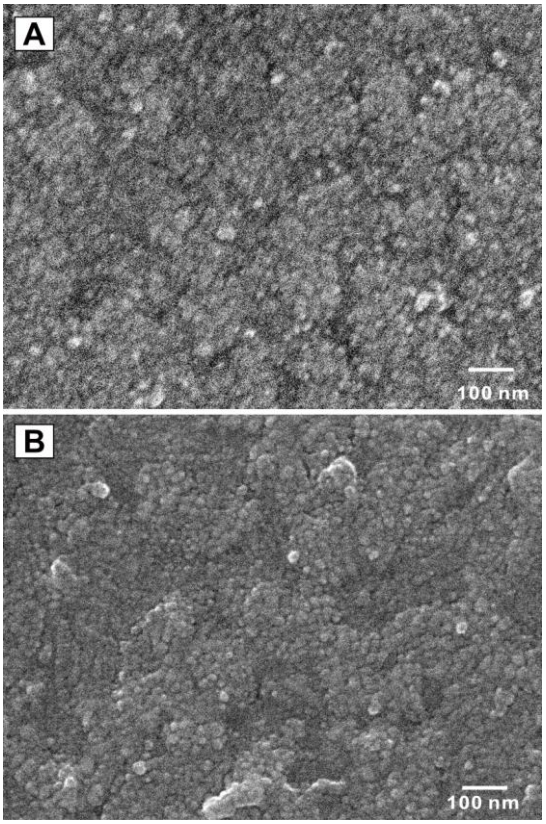

Figure 1. FESEM images of (A) CeHCF(II) nanoparticles and (B) ADH/PLL/CeHCF/PLL film.

The size of CeHCF(II) nanoparticles is from 25 to 30 nm and they possess porous surface morphology. Fig. 1 (B) shows the FESEM image of ADH/PLL/CeHCF/PLL nanocomposite film. ADH has been coated well above the PLL/CeHCF/PLL film surface, which could be attributed to the porous surface morphology of CeHCF(II) nanoparticles and its strong electrostatic interactions with the positively charged PLL film.

Fig. 2 (A) shows the AFM image of PLL film surface containing numerous folding which can facilitate the CeHCF(II) nanoparticles as well as ADH loading.

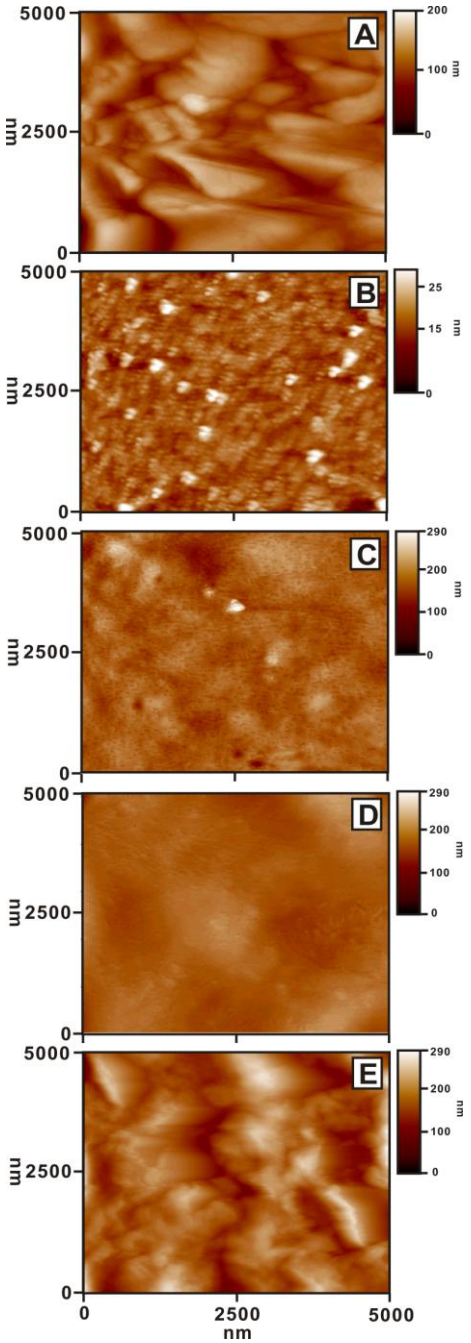

Figure 2. AFM images of (A) PLL, (B) CeHCF(II) nanoparticles, (C) CeHCF/PLL, (D) ADH and (E) ADH/PLL/CeHCF/PLL films.

In contrast, as shown in fig. 2 (B) CeHCF(II) nanoparticles surface possess several bright, spherical shaped particles. Few slightly larger particles are also found on the film surface, which might have formed due to the association of smaller particles. Fig. 2 (C) shows the AFM image of CeHCF/PLL film. Unlike that of fig. 2 (B), individual particles are not clearly seen on the CeHCF/PLL film surface because the nanoparticles should be deeply embedded into the PLL matrix. Fig. 2 (D) shows the ADH film surface with thin surface morphology. On the other hand, fig. 2 (E) shows thick ADH/PLL/CeHCF/PLL nanocomposite film modified surface containing bright fine folded structures. Thus AFM results validate that ADH has been well immobilized at the PLL/CeHCF/PLL nanocomposite film surface.

3.2 Powder XRD studies

Fig. 3 shows the powder XRD pattern of electrochemically prepared CeHCF(II) nanoparticles.

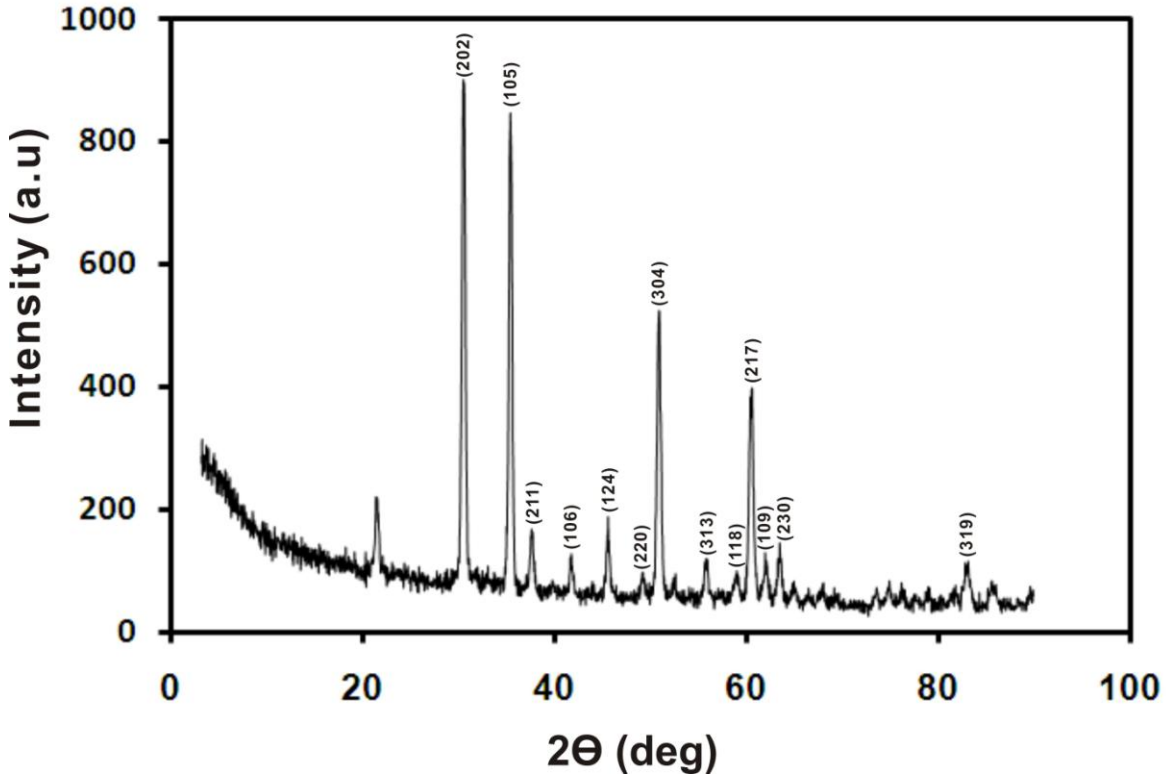

Figure 3. Powder XRD pattern of electrochemically deposited CeHCF(II) nanoparticles.

The peak positions and their relative intensities and the corresponding 2Θ angles are consistent with the standard powder diffraction pattern of $KCe[Fe(CN)_6] \cdot 4H_2O$, (PDF # 83-2292). High intensity peaks are found at (202), (105), (304) and (217) planes which can be assigned to the hexagonal symmetry of $KCe[Fe(CN)_6]. 4H_2O$. Feng et *al.* observed notably high intensity peaks at (101), (102), and (203) planes, from which they confirmed the hexagonal symmetry and the preferential orientation of $KCe[Fe(CN)_6].4H_2O$ structures [24].

3.3 Electrochemical characterization of various film modified GCEs

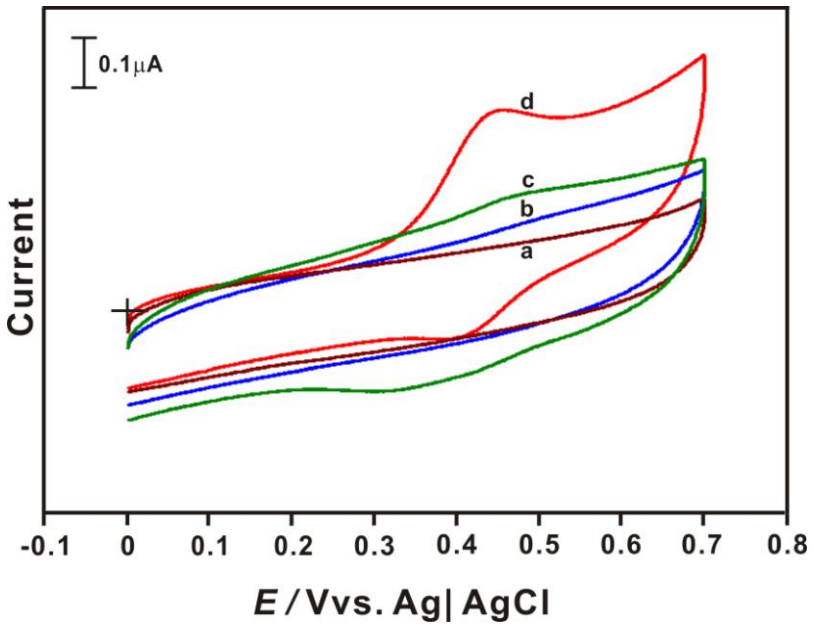

Figure 4. Cyclic voltammograms obtained at (a) PLL, (b) bare, (c) CeHCF/PLL (d) ADH/PLL/CeHCF/PLL nanocomposite film modified GCEs in N_2 saturated 0.1 M KNO_3 solution (pH 7) at the scan rate of 100 mV s^{-1}.

In Fig. 4, curves (a-d) shows the cyclic voltammograms obtained at bare, PLL, CeHCF/PLL and ADH/PLL/CeHCF/PLL modified GCEs at the scan rate of 100 mV s^{-1} in N_2 saturated 0.1 M KNO_3 solution (pH 7). Cyclic voltamograms were recorded in the potential range of 0 to 0.7 V. From fig. 4, it is clear that no significant redox peaks are noticed at both unmodified and PLL modified GCEs. However, CeHCF/PLL/GCE exhibits quasi reversible redox peaks at a formal potential (E°′) of 0.42 V. This result confirms that the redox peaks observed at CeHCF/PLL/GCE belongs to the redox reaction of CeHCF. The anodic peak at 0.38 V corresponds to the oxidation of $Fe(CN)_6^{4-}$ to $Fe(CN)_6^{3-}$ and the cathodic peak observed at 0.46 V could be ascribed to the reduction of $Fe(CN)_6^{3-}$ to $Fe(CN)_6^{4-}$. In order to evaluate the role of PLL in the deposition process, we also fabricated CeHCF(II) nanoparticles on GCE without PLL layer and we investigated its electrochemical behavior under similar experimental conditions in N_2 saturated 0.1 M KNO_3 solution (pH 7) (not shown). However, we observed a steady decrease in peak currents with increased potential sweep cycles, indicating the poor adhering ability of CeHCF film onto GCE. But in the case of PLL/CeHCF/GCE no obvious decrease in peak current and shift in peak positions were observed, which validates the strong interactions between the oppositely charged CeHCF and PLL films. On the other hand, compared with CeHCF/PLL/GCE, ADH/PLL/CeHCF/PLL modified GCE exhibits well defined redox peaks at an E°′ of 0.44 V with much higher redox peaks corresponding to the $Fe(CN)_6^{4-/3-}$ redox process. The appearance of well defined redox peaks with slight negative potential shifts validates the immobilization of ADH at the composite film. Moreover, the enhanced redox peak currents observed at the composite film validates the rapid redox process occurring at the composite film surface, which

could be ascribed to the efficient loading of ADH as well as the good electron transfer ability of CeHCF(II) nanoparticles.

Fig. 5 shows the cyclic voltammograms obtained at ADH/PLL/CeHCF/PLL/GCE in N_2 saturated 0.1 M KNO_3 solution (pH 7) at different scan rates. Both I_{pa} and I_{pc} increased linearly with increase in scan rates between 100–2950 mV s^{-1}, thus the redox process occurring at ADH/PLL/CeHCF/PLL/GCE is surface-confined. The peak currents (I_{pa} and I_{pc}) vs. scan rates plot is shown in fig. 5 inset. Both Ip_a and I_{pc} exhibited linear relationship with scan rates, R^2 = 0.9955 and 0.9384, respectively.

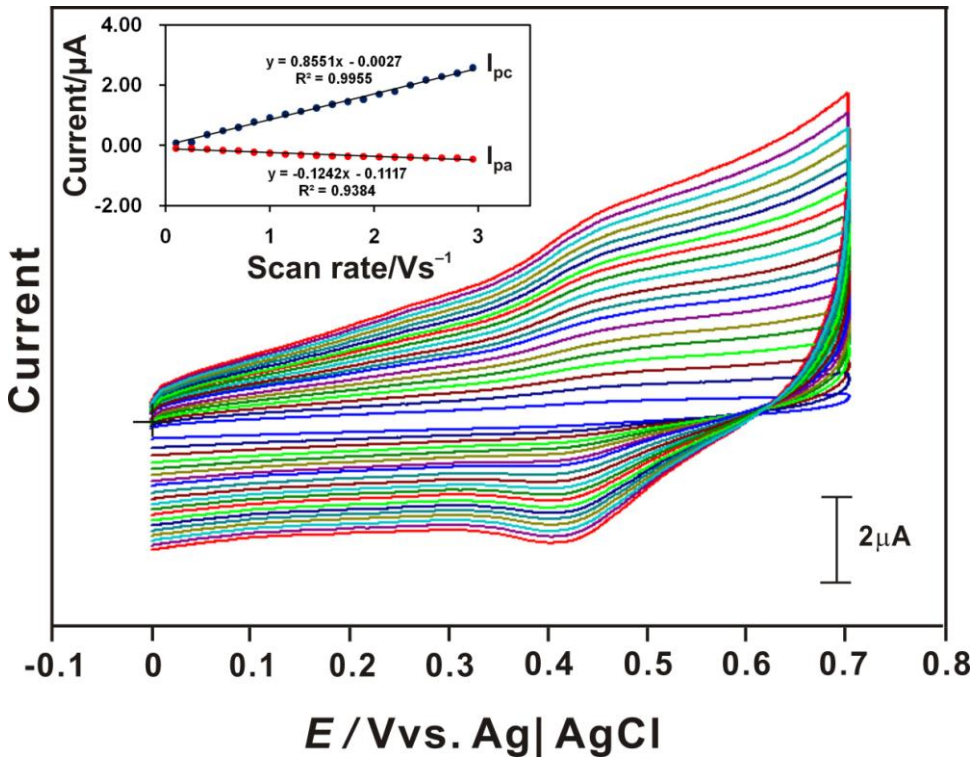

Figure 5. Cyclic voltammograms recorded at ADH/PLL/CeHCF/PLL nanocomposite film in N_2 saturated 0.1 M KNO_3 solution (pH 7) at different scan rates. The scan rates from inner to outer are: 100, 250, 400, 550, 700, 850, 1000, 1150, 1300, 1450, 1600, 1750, 1900, 2050, 2200, 2350, 2500, 2650, 2800 and 2950 mV s^{-1}, respectively. Inset shows the linear dependence of I_{pa} and I_{pc} on scan rate.

3.4 EIS studies at various films

The interfacial changes originating from the biorecognition events at the electrode surfaces can be analyzed through impedance spectroscopy [28, 29]. Fig. 6 (A) shows the real and imaginary parts of the impedance spectra represented as Nyquist plots (Z_{im} vs. Z_{re}) for bare and ADH film modified GCEs obtained in 0.1 M KNO_3 solution (pH 7) containing 5 mM $Fe(CN)_6^{3-/4-}$. Compared with bare/GCE, an enlarged semicircle has been observed at the ADH modified GCE, indicating the sluggish electron transfer process occurring at the later. The poor electron transferring ability of ADH/GCE can be

ascribed to the strong electrostatic repulsive forces offered by the negatively charged ADH film surface towards the $Fe(CN)_6^{3-}$ ions which hinders the diffusion of the later towards the transducer surface.

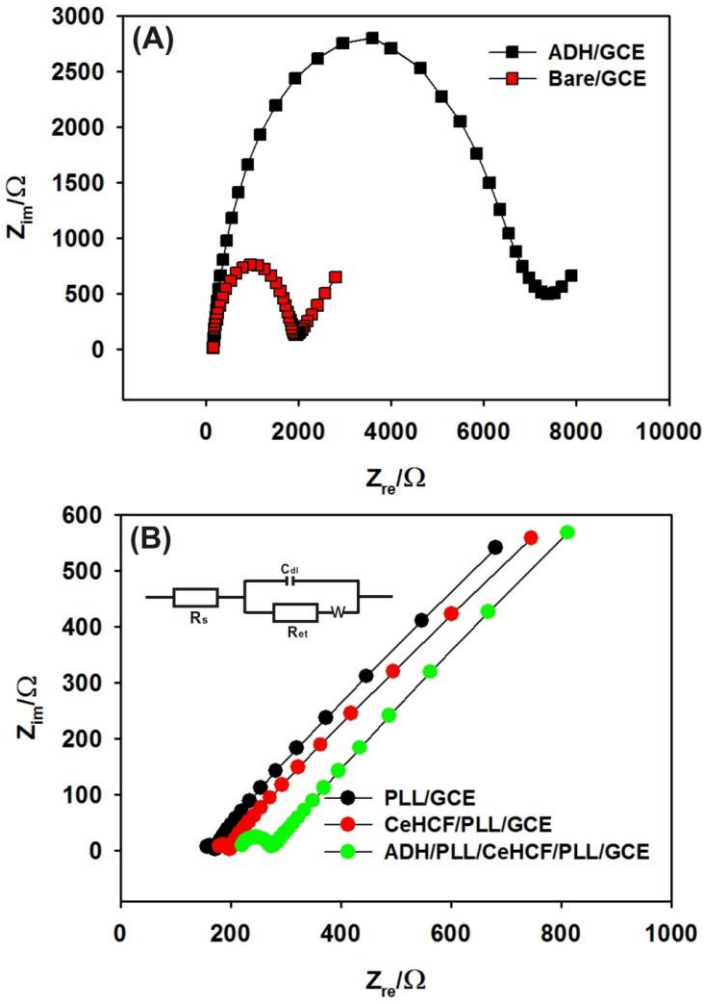

Figure 6. (A) EIS of bare and ADH film modified GCEs recorded in 0.1M KNO_3 solution (pH 7) containing 5 mM $Fe(CN)6^{3-/4-}$. Amplitude: 5 mV, frequency: 100 mHz to 100 kHz. (B) EIS of PLL, CeHCF/PLL and ADH/PLL/CeHCF/PLL film modified GCEs recorded at similar conditions as fig. 6 (A). Inset is the Randles equivalence circuit model used to fit the experimental data.

Fig. 6 (B) shows the Nyquist plots of PLL, CeHCF/PLL and ADH/PLL/CeHCF/PLL modified GCEs recorded at similar conditions as fig. 6 (A). It is clear that all these modified GCEs exhibited depressed semicircles with similar semicircle diameters. Notably, comparing the Nyquist plot of CeHCF/PLL/GCE with PLL/GCE, it is clear that the semicircle portion of the former has been slightly shifted towards higher frequency. However, the semicircle diameter remain unchanged, thus the presence of CeHCF(II) nanoparticles layer sustains the electron transfer process at the CeHCF/PLL/GCE. However, upon the fabrication of PLL and ADH layers the semicircle diameter have augmented slightly for the ADH/PLL/CeHCF/PLL nanocomposite and much lower frequency

shift is also observed, indicating the efficient immobilization of PLL and ADH layers. Thus EIS study has been used as an effective tool to monitor the step-wise film fabrication process on GCE.

3.5 NAD^+ concentration and pH optimization studies

The biosensor response depends up on the concentration of NAD^+ present in the supporting electrolyte solution. Therefore the optimization of NAD^+ concentration is obligatory. Fig. 7 shows the plot of effect of NAD^+ concentrations on the biosensor response towards 0.2 mM ethanol. Cyclic voltammograms were recorded at ADH/PLL/CeHCF/PLL/GCE at the scan rate of 100 mV s^{-1} in the potential range from 0 to 0.7 V (not shown). The NAD^+ concentrations used were 10, 15, 20 and 25 mM and the supporting electrolyte used is N_2 saturated 0.1 M KNO_3 solution (pH 7). The maximum biosensor response was observed in the presence of 20 mM NAD^+ and therefore this optimized NAD^+ concentration (20 mM) have been used for all the electrocatalytic experiments.

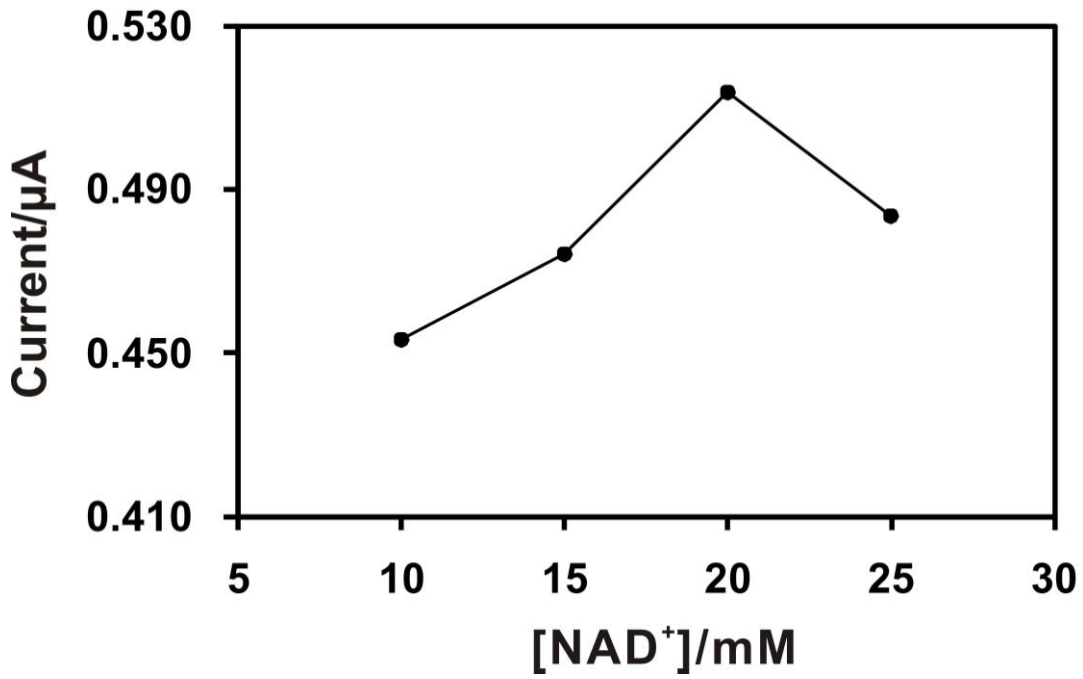

Figure 7. The effect of NAD^+ concentrations on the response of the biosensor towards 0.2 mM ethanol in N_2 saturated 0.1 M KNO_3 solution (pH 7) solution.

Since pH of the supporting electrolyte can influence the biosensor response, it is much requisite to choice the optimum pH for electrocatalytic experiments. Fig. 8 shows the effect of pH on the biosensor response towards 0.2 mM ethanol. It is clear from the plot shown in fig. 8 that maximum biosensor response has been observed in pH 7. Therefore, pH 7 has been chosen as optimum pH for all electrocatalytic ethanol experiments.

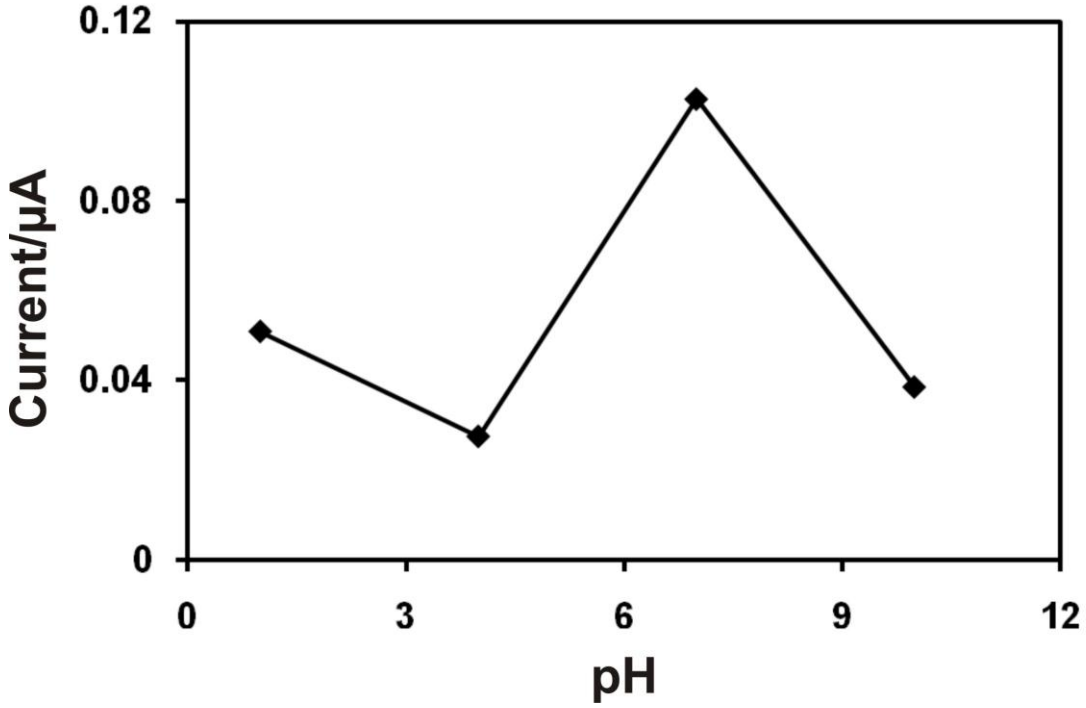

Figure 8. The effect of pH on the response of the biosensor towards 0.2 mM ethanol in N_2 saturated different buffer solutions with pH 1, 4, 7 and 10 containing each 20 mM NAD^+.

3.6 Investigation of electrocatalytic oxidation of ethanol at nanocomposite film modified electrode

Fig. 9 shows the cyclic voltamograms obtained at ADH/PLL/CeHCF/PLL nanocomposite film modified GCE in the presence of various ethanol concentrations in N_2 saturated 0.1 M KNO_3 solution (pH 7) containing 20 mM NAD^+. The potential range used is from 0 to 0.7 V. As shown in fig. 9, an enhanced electrocatalytic oxidation peak is observed at an I_{pa} of 0.502 V for 0.03 mM ethanol. This anodic peak current increased linearly up to 0.67 mM ethanol concentration additions while the cathodic peak current decreased concurrently ((Fig. 9 (b-g)). Where, both the increase in peak current and decrease in over potential are considered as electrocatalysis. However, no significant catalytic oxidation peak is observed at bare GCE even in the presence of highest (0.67 mM) ethanol concentration (fig. 9 (a′)).

CV results confirmed that the nanocomposite film modified GCE exhibits enhanced electrocatalytic activity towards ethanol and it significantly reduces the over potential for ethanol oxidation. From the calibration plot shown in fig. 9 inset, the linear concentration range and sensitivity values are obtained as 0.06 to 0.67 mM and 3.03 μA mM^{-1} cm^{-2}, respectively. The linear regression equation can be written as I (μA) = 0.2396 C (mM) + 0.4101, R^2 = 0.9068. The excellent response of the biosensor towards ethanol could be attributed to the good biocompatibility of the CeHCF/PLL matrix, efficient ADH immobilization and the synergistic effect of the nanocomposite film towards ethanol.

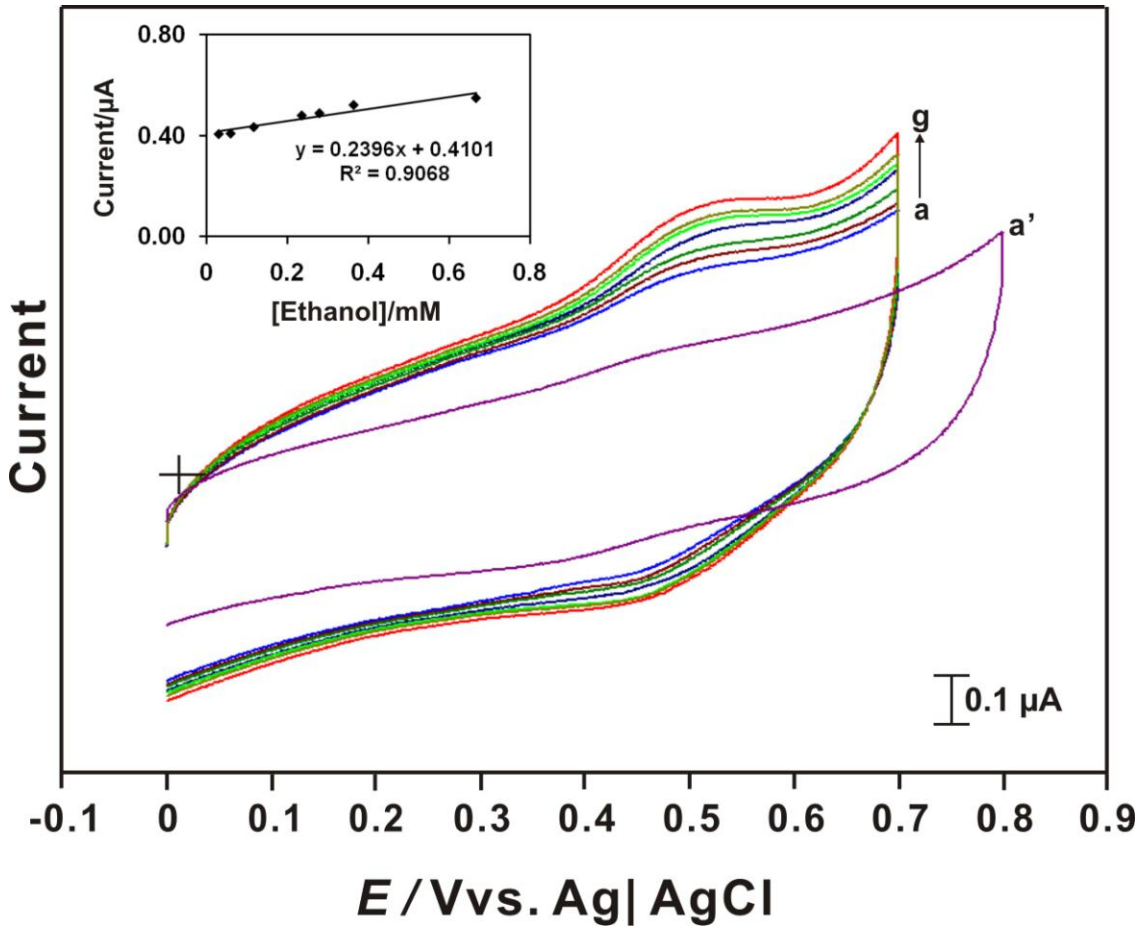

Figure 9. Cyclic voltamograms obtained at ADH/PLL/CeHCF/PLL nanocomposite film modified GCE at the scan rate of 100 mV s^{-1} in the presence of: (a) 0.03, (b) 0.06, (c) 0.12, (d) 0.24, (e) 0.28, (f) 0.36 and (g) 0.67 mM ethanol. (a′) Cyclic voltammogram obtained at bare/GCE in the presence of 0.67 mM ethanol at same conditions. Supporting electrolyte: N_2 saturated 0.1 M KNO_3 solution (pH 7), [NAD^+] used: 20 mM. Inset is the plot of anodic peak current vs. [ethanol]/mM.

3.7. DPV studies for ethanol determination

Electrocatalytic oxidation of ethanol in acidic [30, 31], alkaline [32] or near neutral [14] pH has been studied widely using voltammetry technique. Since, DPV technique is highly sensitive we have used DPV technique to investigate the biosensor activity towards ethanol. During DPV experiments, to achieve uniform mixing of analyte with the supporting electrolyte solution, after each successive ethanol concentration additions pre-purified N_2 gas was purged into the supporting electrolyte solution for 1 min. In Fig. 10, curve (a) represents the differential pulse voltammogram obtained at ADH/PLL/CeHCF/PLL nanocomposite film in the absence of ethanol in 0.1M KNO_3 solution (pH 7).

Whereas curves (b-f) represents the differential pulse voltammograms obtained at the nanocomposite film in the presence of various ethanol concentration additions in to 0.1 M KNO_3 solution (pH 7) containing 20 mM NAD^+. The catalytic oxidation peak current increases linearly with increase in ethanol concentration. From the inset plot, sensitivity and correlation coefficient values are

obtained as 13.86 μA mM^{-1} cm^{-2} and 0.9986, respectively. The linear regression equation can be written as I (μA) = 1.0951 C (mM) + 1.4065, R^2 = 0.9986.

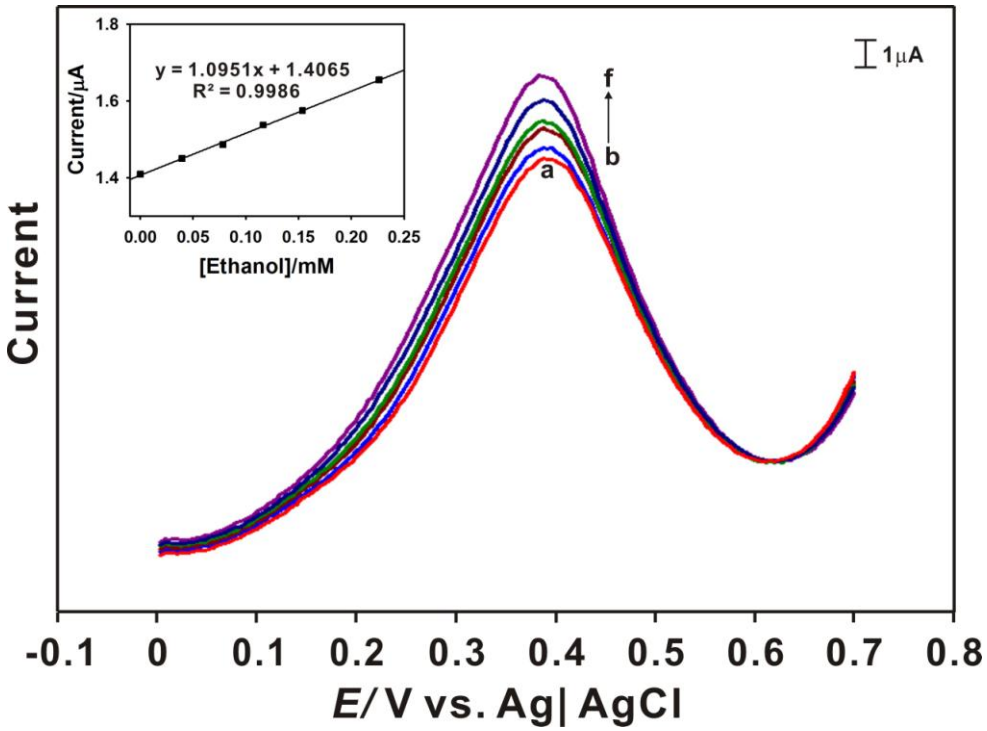

Figure 10. Differential pulse voltammograms obtained at ADH/PLL/CeHCF/PLL nanocomposite film in the absence (a) and presence of (b) 0.04, (c) 0.08, (d) 0.12, (e) 0.15 and (f) 0.23 mM ethanol. Supporting electrolyte: N_2 saturated 0.1 M KNO_3 solution (pH 7), [NAD^+] used: 20 mM. Inset is the plot of anodic peak current vs. [ethanol]/mM.

3.8 Stability and selectivity studies

In order to ascertain the stability of the biosensor, cyclic voltammogramms were continuously recorded at ADH/PLL/CeHCF/PLL film in N_2 saturated 0.1 M KNO_3 solution (pH 7), the background current and peak potentials were monitored after 1st, 100th and 150th cycles. As shown in Fig. 11, no notable decrease in peak currents and peak potential shifts was observed at the ADH/PLL/CeHCF/PLL nanocomposite film even after performing 150 cycles, which validates the good stability of the nanocomposite film. In addition, the biosensor retains 98.4 % of its I_{pa} value even after one week storage in 0.1 M KNO_3 solution (pH 7) at 4°C, which shows its acceptable storage stability. The good storage stability of the biosensor could be attributed to the strong electrostatic interactions between the oppositely charged ADH, PLL and CeHCF(II) nanoparticles layers.

The selectivity of the biosensor is mandatory for practical applications. So we evaluated the selectivity of the biosensor in presence of common interferences such as methanol, propanol, ascorbic acid (AA), dopamine (DA) and uric acid (UA) using DPV technique. Differential pulse voltammogram was recorded at ADH/PLL/CeHCF/PLL/GCE upon adding 0.25 mM ethanol in to 20 mM NAD^+ containing 0.1 M KNO_3 solution (pH 7). The I_{pa} value has been calculated and the activity of the

biosensor has been considered as 100 (%). The effect of interferences has been evaluated from the variation between I_{pa} values of ethanol before and after adding the above stated common interfering species in to the same supporting electrolyte solution. These interference values are given as activity (%) in Table 1. Among these results, the presence of methanol and DA decreased the activity (%) of ethanol where as the presence of other analytes increased the activity (%) of ethanol. The selectivity results thus reveals that ADH/PLL/CeHCF/PLL film has good anti-interfering ability and it can be employed for real sample applications.

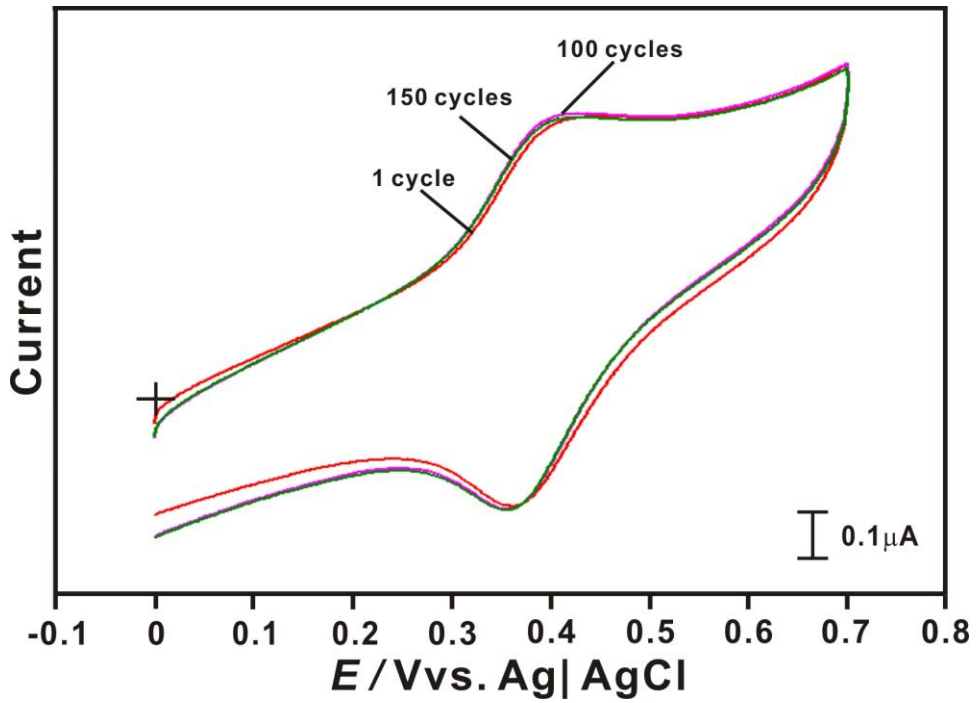

Figure 11. 1st, 100th and 150th cycles obtained at ADH/PLL/CeHCF/PLL nanocomposite film in N_2 saturated 0.1 M KNO_3 solution (pH 7).

Table 1. Selectivity study results obtained at ADH/PLL/CeHCF/PLL nanocomposite film modified GCE

Analyte	[Analyte]/mM	Activity (%)
Methanol	0.25	-16.7
Propanol	0.13	4.13
Ascorbic acid	0.19	4.89
Uric acid	0.25	1.62
Dopamine	0.19	-12.6

3.9 Real sample analysis

The practical applicability of the proposed biosensor has been corroborated through real sample analysis. The technique used is DPV. Commercially available red wine containing 12.5 % ethanol was purchased from local departmental store in Taipei, Taiwan. Further dilutions were done using 0.1 M KNO_3 solution (pH 7). From the amount of added and found ethanol concentrations, recovery has been calculated and the results are given in Table 2.

Table 2. Electroanalytical results obtained at ADH/PLL/CeHCF/PLL nanocomposite film modified GCE for the determination of ethanol from red wine

Added (mM)	Found (mM)	Recovery (%)
0.120	0.116	96.7
0.150	0.153	102.0
0.230	0.236	102.6

The determination of ethanol from red wine with good recovery shows the practical applicability of the biosensor for ethanol quantification.

4. CONCLUSIONS

We fabricated an ethanol biosensor using nanocomposite film containing CeHCF(II) nanoparticles, PLL and ADH. The conductive CeHCF layer has been sandwiched between biocompatible PLL layers and the resulting nanocomposite film has been used as a novel immobilization matrix for ADH. The electrostatic interactions between the oppositely charged CeHCF(II) nanoparticles, PLL and ADH provide good stability to the nanocomposite. Moreover, the porous surface morphology of CeHCF(II) nanoparticles and folded surface morphology of PLL are beneficial for achieving efficient ADH immobilization. The proposed biosensor is highly selective towards ethanol present in lab and red wine samples.

ACKNOWLEDGEMENT

This work was supported by the National Science Council of the Taiwan (ROC).

References

1. M. Rocchia, M. Ellena, G. Zeppa, *J. Agric. Food Chem*., 55 (2007) 5984.
2. L.D. Mello, L.T. Kubota, *Food Chem*., 77 (2002) 237.
3. P.C. Pandey, S. Upadhyay, I. Tiwari, V.S. Tripathi, *Electroanalysis*, 13 (2001) 820.
4. Q. Yao, S. Yabuki, F. Mizutani, *Sens. Actuators* B, 65 (2000) 147.
5. Y. Liu, F. Yin, Y. Long, Z. Zhang, S. Yao, *J. Colloid Interface Sci*., 258 (2003) 75.

6. C. Lee, Y. Tsai, *Sens. Actuators* B, 138 (2009) 518.
7. M. Piao, D. Yang, K. Yoon, S. Lee, S. Choi, *Sensors,* 9 (2009) 1662.
8. B. Grundig, G. Wittstock, U. Rudel, B. Strehlitz, *J. Electroanal. Chem*., 395 (1995) 143.
9. R. Yuan, S. Kuwabata, H. Yoneyama, *Chem. Lett*., (1996) 137.
10. C.X. Cai, K.H. Xue, Y.M. Zhou, H. Yang, *Talanta,* 44 (1997) 339.
11. A.S. Santos, A.C. Pereira, N. Duran, L.T. Kubota, *Electrochim. Acta*, 52 (2006) 215.
12. L. Meng, P. Wu, G. Chen, C. Ca, *J. Electrochem. Soc*., 155 (2008) F231.
13. P. Du, S. Liu, P. Wu, C. Cai, *Electrochim. Acta,* 53 (2007) 1811.
14. A.P. Periasamy, Y. Umasankar, S.M. Chen, *Talanta*, 83 (2011) 930.
15. S.J. Reddy, A. Dostal, F. Scholz, J. *Electroanal. Chem*., 403 (1996) 209.
16. U, Schro1der and F. Scholz, *Inorg. Chem*., 39 (2000) 1006.
17. P. Wu, S. Lu, C. Cai, *J. Electroanal. Chem*., 569 (2004) 143.
18. P.G. Fenga, N.R. Stradiotto, M.I. Pividori, *Electroana*l., 23 (2011) 1100.
19. H. Yu, S.W. Song, Y.Y. Lian, Z.Y. Liu, G.C. Qi, *J. Electroanal. Chem*., 650 (2010) 82.
20. Y. Liu and L. Xu, *Sensors*, 7(2007) 2446.
21. H. Razmi, A. Taghvimi, *Int. J. Electrochem. Sci*., 5 (2010) 751.
22. M. Yang, J. Jiang, Y. Yang, X. Chen, G. Shen, R. Yu, *Biosens. Bioelectron*., 21 (2006) 1791.
23. A.P. Baioni, M. Vidotti, P.A. Fiorito, S.I.C.D Torresi, *J. Electroanal. Chem*., 622 (2008) 219.
24. L.D. Feng, M.M. Gu, Y.L. Yang, G.X. Liang, J.R. Zhang, J.J. Zhu, *J. Phys. Chem*. C, 113 (2009) 8743.
25. H. Yang, B. Lu, L. Guo, B. Qi, *J. Electroanal. Chem*., 650 (2011) 171.
26. C. Jiang, T. Yang, K.Jiao, H. Gao, *Electrochim. Acta*, 53 (2008) 2917.
27. Liu S, Cai, C, *J. Electroanal. Chem*., 602 (2007) 103.
28. E. Katz, I. Willner, *Electroanal*., 15 (2003) 913.
29. P.A. Prakash, U. Yogeswaran, S.M. Chen, *Talanta*, 78 (2009) 1414.
30. H. Li, D. Kang, H. Wang, R. Wang, *Int. J. Electrochem. Sci.*, 6 (2011) 1058.
31. Y. Umasankar, A.P. Periasamy, S.M. Chen, *Talanta,* 80 (2010) 1094.
32. R.M. Piasentin, E.V. Spinace, M.M. Tusi, A.O. Neto, *Int. J. Electrochem. Sci.*, 6 (2011) 2255.